Significantly reduced thermal conductivity in β-$(Al_{0.1}Ga_{0.9})_2O_3/Ga_2O_3$ superlattices

Cite as: Appl. Phys. Lett. **115**, 092105 (2019); doi: 10.1063/1.5108757
Submitted: 1 May 2019 · Accepted: 27 July 2019 ·
Published Online: 27 August 2019

View Online

Export Citation

CrossMark

Zhe Cheng,[1] Nicholas Tanen,[2] Celesta Chang,[3] Jingjing Shi,[1] Jonathan McCandless,[4] David Muller,[5,6] Debdeep Jena,[2,4,6] Huili Grace Xing,[2,4,6] and Samuel Graham[1,7,a)]

AFFILIATIONS

[1]George W. Woodruff School of Mechanical Engineering, Georgia Institute of Technology, Atlanta, Georgia 30332, USA
[2]Department of Materials Science and Engineering, Cornell University, Ithaca, New York 14853, USA
[3]Department of Physics, Cornell University, Ithaca, New York 14853, USA
[4]School of Electrical and Computer Engineering, Cornell University, Ithaca, New York 14853, USA
[5]School of Applied and Engineering Physics, Cornell University, Ithaca, New York 14853, USA
[6]Kavli Institute for Nanoscale Science, Cornell University, Ithaca, New York 14853, USA
[7]School of Materials Science and Engineering, Georgia Institute of Technology, Atlanta, Georgia 30332, USA

[a)]Author to whom correspondence should be addressed: sgraham@gatech.edu

ABSTRACT

β-Ga_2O_3 has emerged as a promising candidate for electronic device applications because of its ultrawide bandgap, high breakdown electric field, and large-area affordable substrates grown from the melt. However, its thermal conductivity is at least one order of magnitude lower than that of other wide bandgap semiconductors such as SiC and GaN. Thermal dissipation in electronics made from β-Ga_2O_3 will be the bottleneck for real-world applications, especially for high power and high frequency devices. Similar to AlGaN/GaN interfaces, β-$(Al_xGa_{1-x})_2O_3/Ga_2O_3$ heterogeneous structures have been used to form a high mobility two-dimensional electron gas where joule heating is localized. The thermal properties of β-$(Al_xGa_{1-x})_2O_3/Ga_2O_3$ are the key for heat dissipation in these devices, while they have not been studied before. This work reports the temperature dependent thermal conductivity of β-$(Al_{0.1}Ga_{0.9})_2O_3/Ga_2O_3$ superlattices from 80 K to 480 K. Its thermal conductivity is significantly reduced (5.7 times reduction) at room temperature compared to that of bulk Ga_2O_3. Additionally, the thermal conductivity of bulk Ga_2O_3 with (010) orientation is measured and found to be consistent with literature values regardless of Sn doping. We discuss the phonon scattering mechanism in these structures by calculating their inverse thermal diffusivity. By comparing the estimated thermal boundary conductance (TBC) of β-$(Al_{0.1}Ga_{0.9})_2O_3/Ga_2O_3$ interfaces and Ga_2O_3 maximum TBC, we reveal that some phonons in the superlattices transmit through several interfaces before scattering with other phonons or structural imperfections. This study is not only important for Ga_2O_3 electronics applications, especially for high power and high frequency applications, but also for the fundamental thermal science of phonon transport across interfaces and in superlattices.

Published under license by AIP Publishing. https://doi.org/10.1063/1.5108757

As an emerging ultrawide bandgap semiconductor material, β-Ga_2O_3 has shown promising properties for electronic device applications, such as an ultrawide bandgap (4.8 eV) and high critical electric field (8 MV/cm), which results in a Baliga figure of merit that is 3214 times that of Si.[1] However, the thermal conductivity of bulk β-Ga_2O_3 (10–30 W/m-K, depending on crystal orientation) is at least one order of magnitude lower than those of other wide bandgap semiconductors such as GaN (230 W/m-K), 4H-SiC (490 W/m-K), and diamond (>2000 W/m-K).[2,3] Thermal dissipation will be the bottleneck for real-world applications, especially for high power and high frequency devices. Currently, compared to demonstrations of Ga_2O_3 devices, a disproportionately smaller number of thermal studies have been performed.[4] Similar to AlGaN/GaN interfaces, to demonstrate modulation-doped field effect transistors (MODFETs), β-$(Al_xGa_{1-x})_2O_3/Ga_2O_3$ heterogeneous structures have been used to form a high mobility two-dimensional electron gas (2DEG) where joule heating is localized.[5–9] The thermal properties of the β-$(Al_xGa_{1-x})_2O_3/Ga_2O_3$ structure are the key for heat dissipation in these devices; however, they have not been studied before.

In this work, we report the temperature dependent thermal conductivity of β-$(Al_{0.1}Ga_{0.9})_2O_3/Ga_2O_3$ superlattices epitaxially grown on bulk (010) Ga_2O_3 substrates by molecular-beam epitaxy (MBE) from 80 K to 480 K. Multifrequency time-domain thermoreflectance (TDTR) is used to measure the thermal properties of both the β-$(Al_{0.1}Ga_{0.9})_2O_3/Ga_2O_3$ superlattices and the bulk Ga_2O_3 substrates simultaneously. The phonon scattering mechanism in these structures is discussed in detail. Additionally, we estimate the thermal boundary conductance (TBC) of β-$(Al_{0.1}Ga_{0.9})_2O_3/Ga_2O_3$ interfaces and compare it with that of maximum Ga_2O_3 TBC. The mechanism of phonons transmission through interfaces is discussed.

The β-$(Al_xGa_{1-x})_2O_3/Ga_2O_3$ superlattice used in this study was homoepitaxy-grown on a Sn-doped (010) Ga_2O_3 substrate, with an n-type doping concentration of 4×10^{18} cm^{-3}, using a Veeco Gen930 MBE system. The aluminum and gallium were provided by standard effusion cells. The oxygen plasma was produced using a Veeco RF plasma source. During the growth, the gallium and aluminum beam equivalent pressures (BEPs) measured using an ion gauge were 1×10^{-8} Torr and 1×10^{-9} Torr, respectively. This led to an aluminum flux that is 9.1% of the total metal flux. The oxygen was flown into the chamber at 0.7 sccm, and the RF plasma was struck using a load power of 289 W, which corresponded to a total chamber pressure of 2.18×10^{-5} Torr. The substrate temperature, measured using a thermocouple, was 500 °C for the entire growth. The substrate was mounted to a silicon carrier wafer using indium bonding. The substrate was grown by edge-defined film-fed growth (EFG) purchased from Novel Crystal Technology. The film has ten alternating periods of a Ga_2O_3 layer followed by a $(Al_{0.1}Ga_{0.9})_2O_3$ layer each grown for 30 min.

A cross-sectional TEM specimen was prepared using an FEI Strata 400 Focused Ion Beam (FIB) with a final milling step of 5 keV to reduce surface damage. Atomic resolution high angle annular dark field (HAADF) images were acquired on an aberration corrected 300 keV Themis Titan. The superlattice film thickness was determined by scanning transmission electron microscopy (STEM) to be 114 nm, as shown in Fig. 1. For each period, the Ga_2O_3 layer is 6.5 nm (±0.2 nm) thick, while the $(Al_{0.1}Ga_{0.9})_2O_3$ layer is 4.5 nm (±0.1 nm) thick. The interfaces in the superlattice structure are not very sharp. A layer of Al (~80 nm) was deposited on the surface as the TDTR transducer as demonstrated in several previous studies.[10–14] A modulated pump beam heats the sample surface periodically, while a delayed probe beam detects the surface temperature variation via thermoreflectance. The measured signal of temperature variation is fit with an analytical heat transfer solution to infer unknown parameters. Here, we measure one spot on the sample with two modulation frequencies, i.e., 3.6 MHz and 8.8 MHz, at room temperature. The TDTR signal is sensitive to the thermal conductivity of the bulk Ga_2O_3 substrate with a modulation frequency of 3.6 MHz, while it is sensitive to the thermal conductivity of the superlattice with a modulation frequency of 8.8 MHz. More details about multifrequency TDTR measurements can be found in references and the supplementary material.[10,15–17] The estimate of volumetric heat capacity of the superlattice is shown in the supplementary material. Additionally, we estimate the error bars here to be ±10%.

The temperature-dependent thermal conductivities of the bulk (010) Ga_2O_3 substrate and the β-$(Al_{0.1}Ga_{0.9})_2O_3/Ga_2O_3$ superlattice are shown in Fig. 2(a). At room temperature, the thermal conductivity of the superlattice is 5.7 times smaller than that of the bulk (010) Ga_2O_3 substrate. This significantly reduced thermal conductivity further impedes thermal dissipation, potentially creating additional challenges for gallium oxide electronics devices. Aggressive thermal management techniques need to be applied for reliable device performance, such as integrating high thermal conductivity materials close to the regions where heat is being generated to aid in conducting and spreading the heat away from the source location. For the bulk (010) Ga_2O_3 substrate, its thermal conductivity decreases with increasing temperature from 80 K to 450 K because of increased phonon-phonon scattering. As temperature increases, the number of excited phonons increases, resulting in increasingly extensive phonon-phonon scattering. For the superlattice, its thermal conductivity shows a peak at 380 K. Below 380 K, the thermal conductivity decreases with decreasing temperature, while it decreases with increasing temperature above 380 K. For temperatures below 380 K, phonon-structural imperfection scattering, such as alloy and boundary, dominates in impeding thermal transport. The thermal conductivity of superlattices can be reduced to be lower than their amorphous counterparts due to the large number of thermal boundary resistances, especially when the boundaries are composed of two dissimilar materials which have very low TBC.[18] For temperatures above 380 K, phonon-phonon scattering dominates. More about the scattering mechanisms will be discussed later.

The measured thermal conductivity of the bulk (010) Ga_2O_3 substrate is compared with literature values as shown in Fig. 2(b). Our measured values are consistent with most of the other experimentally

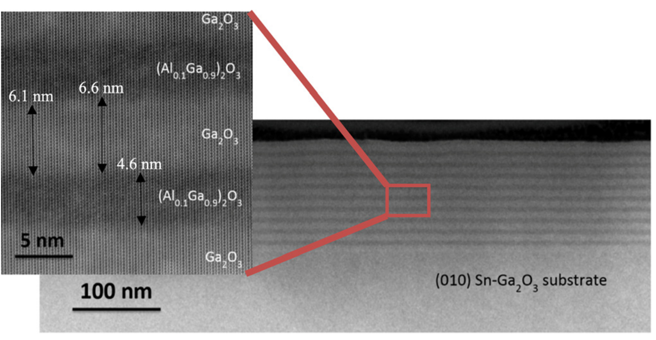

FIG. 1. HAADF-STEM images of the β-$(Al_{0.1}Ga_{0.9})_2O_3/Ga_2O_3$ superlattice structure.

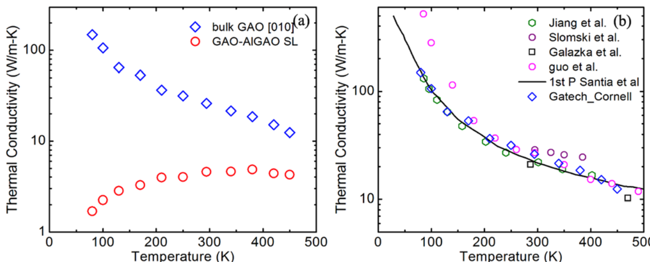

FIG. 2. (a) Temperature-dependent thermal conductivity of the bulk Ga_2O_3 substrate and β-$(Al_{0.1}Ga_{0.9})_2O_3/Ga_2O_3$ superlattices. (b) Summary of temperature-dependent thermal conductivity of bulk (010) β-Ga_2O_3 in this work and the literature.[3,19,20]

Published under license by AIP Publishing

measured values and first-principles calculated values in the literature. This indicates that the Sn doping and unintentional doping do not affect the thermal conductivity significantly. The other samples measured in the literature have different levels of doping as well. It is still an open question as to how high doping concentrations impact the thermal conductivity in β-Ga_2O_3.

To better understand the phonon scattering mechanism in the superlattice and bulk Ga_2O_3, we calculate the inverse thermal diffusivity of both the superlattice and bulk Ga_2O_3, as shown in Fig. 3(a). The formula of inverse thermal diffusivity is shown as follows:

$$\frac{C_v}{k}(T) = \left\{ \sum_{n=1}^{n} \int_0^{\omega_D} g(\omega) k_B \left(\frac{\hbar\omega}{k_B T}\right)^2 e^{\frac{\hbar\omega}{k_B T}} \Big/ \left(e^{\frac{\hbar\omega}{k_B T}} - 1\right)^2 d\omega \right\} \Big/ \left\{ \sum_{n=1}^{n} \int_0^{\omega_D} g(\omega) k_B \left(\frac{\hbar\omega}{k_B T}\right)^2 e^{\frac{\hbar\omega}{k_B T}} \Big/ \left(e^{\frac{\hbar\omega}{k_B T}} - 1\right)^2 v_\omega^2 \left(\frac{1}{\tau_{ph}} + \frac{1}{\tau_{struc}}\right)^{-1} d\omega \right\}. \quad (1)$$

Here, C_v is the volumetric heat capacity, k is the thermal conductivity, T is the temperature, n is the number of phonon branches, ω_D is the Debye frequency, $g(\omega)$ is the phonon density of states, k_B is the Boltzmann constant, $\hbar$ is the reduced Planck constant, ω is the phonon frequency, v_ω is the phonon group velocity, τ_{ph} is the relaxation time for phonon-phonon scattering, and τ_{struc} is the relaxation time for phonon-structural imperfection scattering. To the first-order approximation, the inverse thermal diffusivity can be used to estimate the relative contribution of scattering sources.[21–23] The temperature-dependent thermal conductivities of the superlattice and bulk Ga_2O_3 have different trends from temperature. The strong temperature dependence of heat capacity makes it difficult to compare the contribution of phonon-phonon scattering and phonon-structural imperfection scattering according to the thermal conductivity data. After removing the effect of heat capacity, the inverse thermal diffusivity represents the relative contributions of phonon scattering sources qualitatively. As shown in Fig. 3(a), the inverse thermal diffusivity decreases with decreasing temperature because of reduced scattering intensity of phonon-phonon scattering. As temperature reaches zero, phonon-phonon scattering diminishes and only structural imperfection scattering remains. Then, Eq. (1) can be simplified as

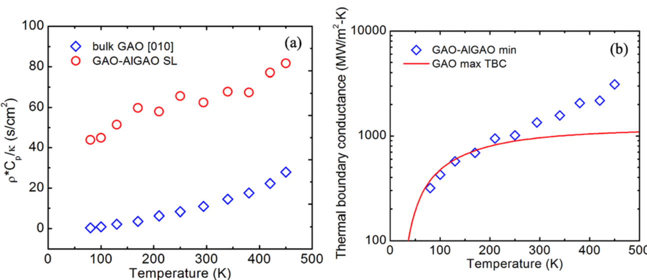

FIG. 3. (a) Temperature-dependent inverse thermal diffusivity of bulk (010) Ga_2O_3 and β-$(Al_{0.1}Ga_{0.9})_2O_3/Ga_2O_3$ superlattices. (b) Temperature dependence of estimated minimum TBC (lower bound) of β-$(Al_{0.1}Ga_{0.9})_2O_3$ and Ga_2O_3 interfaces and maximum TBC of Ga_2O_3.

$$\frac{C_v}{k}(T \to 0\,\mathrm{K}) \approx \frac{3}{v_0^2 \tau_{struc}} = \frac{3}{v_0 l_0}. \quad (2)$$

Here, v_0 is the average phonon group velocity and l_0 is the scattering length arising from structural imperfections. For the bulk Ga_2O_3, the structural imperfection is negligible, and so nearly zero residual value is observed at low temperatures. However, a large residual value is observed at low temperatures for the superlattice, indicating strong structural imperfection scattering, such as alloy scattering, boundary scattering, and point defect scattering. We estimate the average acoustic phonon group velocity to be 2420 m/s.[20] Based on the residual inverse thermal diffusivity (40 s/cm^2), the structural scattering length l_0 is found to be 3.1 nm, which is close to the layer thickness of the superlattice by considering additional alloy scattering. The rough interfaces in the superlattice may reduce the effective thermal conductivity because the roughness at the interfaces may induce additional phonon scattering.[24]

To understand the mechanism of phonon transmission through $(Al_{0.1}Ga_{0.9})_2O_3/Ga_2O_3$ interfaces, we estimate the TBC as follows:

$$R_0 + \frac{n}{TBC} = \frac{114\,\mathrm{nm}}{k_{measured}}. \quad (3)$$

Here, R_0 is the superlattice thermal resistance of $(Al_{0.1}Ga_{0.9})_2O_3/Ga_2O_3$ interfaces and n is the number of $(Al_{0.1}Ga_{0.9})_2O_3/Ga_2O_3$ interfaces in the sample.[25] TBC in this case refers to the TBC of the $(Al_{0.1}Ga_{0.9})_2O_3/Ga_2O_3$ interface. $k_{measured}$ is the measured effective thermal conductivity of the superlattice. R_0 is supposed to be higher than the thermal resistance of pure Ga_2O_3 with the same thickness.[10,26,27] Here, we only consider the size effect resulting from the total superlattice thickness (114 nm). The thermal conductivity of Ga_2O_3 reduces to 45% according to first-principles calculations.[20] As a result, the minimum TBC of the $(Al_{0.1}Ga_{0.9})_2O_3/Ga_2O_3$ interface could be estimated by assuming R_0 as the thermal resistance of a 114-nm-thick pure Ga_2O_3 layer. To compare with this estimated TBC, we also calculate the max TBC of any heterogeneous interfaces which involve Ga_2O_3. This max TBC is calculated by assuming the phonon transmission coefficient across the interface as unity (all phonons from Ga_2O_3 could transmit through the interface). The definition of TBC can be described as follows:[28,29]

$$G = \frac{1}{4} \sum_j \int v_w c_w t_w dw_j. \quad (4)$$

Here, v_w, c_w, and t_w are the phonon group velocity, heat capacity per frequency, and transmission probability on one side of the interface for polarization j.[29] Max TBC is the value of G when t_w is unity. As shown in Fig. 3(b), the estimated minimum TBC is larger than the max TBC of Ga_2O_3 interfaces, especially at high temperatures. At 450 K, the minimum TBC is almost three times larger than the max Ga_2O_3 TBC. This means that some phonons transmit through several interfaces before scattering with other phonons or structural imperfections. At low temperatures, the minimum TBC should be much larger than the max TBC because phonon mean free paths at low temperatures are much larger than that at room temperature. Phonons could transmit through more interfaces without scatterings. But we overestimate the thermal conductivity of the superlattice at low temperatures significantly, resulting in a small minimum TBC. Here, the estimated TBC is the thermal energy transmitted across the interface for a certain

Published under license by AIP Publishing

temperature difference per unit area. Because the period of the superlattice is very small compared to some long mean free path phonons, some phonons could transmit across several interfaces without scattering with other phonons and structural imperfections. The energies of these phonons are accounted repeatedly several times, resulting in a very large effective TBC, even larger than the max TBC that Ga_2O_3 heterointerfaces could achieve. This nonlocal and nonequilibrium phonon transport across interfaces is one of the challenges to define local temperature and understand thermal transport across interfaces. A similar phenomenon was observed in AlN-GaN superlattices before.[30] Our work is important since it may be necessary to design the superlattices not only for the creation of the channel 2DEG but also for more efficient phonon dissipation through the structure. This electrothermal codesign is truly an important feature for future wide bandgap devices which require enhancements in heat dissipation within the devices.

In summary, this work reports the temperature-dependent measurement on thermal conductivity of β-$(Al_{0.1}Ga_{0.9})_2O_3/Ga_2O_3$ superlattices from 80 K to 480 K. We observed significantly reduced thermal conductivity (5.7 times reduction) at room temperature compared to bulk Ga_2O_3. The thermal conductivity of bulk (010) Ga_2O_3 is measured and found to be consistent with literature values. By calculating the inverse thermal diffusivity of both the superlattice and bulk Ga_2O_3, we qualitatively identify the relative contribution of scattering intensity of phonon-phonon scattering and phonon-structural imperfection scattering. We estimated the scattering length to be 3.1 nm, which is close to the layer thickness of the superlattice by considering additional alloy scattering. The estimated minimum TBC of β-$(Al_{0.1}Ga_{0.9})_2O_3/Ga_2O_3$ interfaces is found to be larger than the Ga_2O_3 maximum TBC. This result shows that some phonons could transmit through several interfaces before scattering with other phonons or structural imperfections. This study is not only important for Ga_2O_3 electronics applications, especially for high power and high frequency applications, but also for the fundamental thermal science of phonon transport across interfaces and in superlattices.

See the supplementary material for the TDTR data fitting process and the estimate of superlattice heat capacity.

The authors would like to acknowledge the funding support from the Air Force Office of Scientific Research under a MURI program (Grant No. FA9550-18-1-0479), a Center of Excellence program (Grant No. FA9550-18-1-0529), and the Office of Naval Research under a MURI program (Grant No. N00014-18-1-2429).

REFERENCES

[1] M. Higashiwaki and G. H. Jessen, Appl. Phys. Lett. **112**, 060401 (2018).
[2] S. Pearton, J. Yang, P. H. Cary IV, F. Ren, J. Kim, M. J. Tadjer, and M. A. Mastro, Appl. Phys. Rev. **5**, 011301 (2018).
[3] P. Jiang, X. Qian, X. Li, and R. Yang, Appl. Phys. Lett. **113**, 232105 (2018).
[4] S. B. Reese, T. Remo, J. Green, and A. Zakutayev, Joule **3**, 903 (2019).
[5] S. Krishnamoorthy, Z. Xia, C. Joishi, Y. Zhang, J. McGlone, J. Johnson, M. Brenner, A. R. Arehart, J. Hwang, and S. Lodha, Appl. Phys. Lett. **111**, 023502 (2017).
[6] Y. Zhang, A. Neal, Z. Xia, C. Joishi, J. M. Johnson, Y. Zheng, S. Bajaj, M. Brenner, D. Dorsey, and K. Chabak, Appl. Phys. Lett. **112**, 173502 (2018).
[7] E. Ahmadi, O. S. Koksaldi, X. Zheng, T. Mates, Y. Oshima, U. K. Mishra, and J. S. Speck, Appl. Phys. Express **10**, 071101 (2017).
[8] T. Oshima, Y. Kato, N. Kawano, A. Kuramata, S. Yamakoshi, S. Fujita, T. Oishi, and M. Kasu, Appl. Phys. Express **10**, 035701 (2017).
[9] Y. Zhang, C. Joishi, Z. Xia, M. Brenner, S. Lodha, and S. Rajan, Appl. Phys. Lett. **112**, 233503 (2018).
[10] Z. Cheng, T. Bougher, T. Bai, S. Y. Wang, C. Li, L. Yates, B. Foley, M. S. Goorsky, B. A. Cola, and F. Faili, ACS Appl. Mater. Interfaces **10**(5), 4808–4815 (2018).
[11] D. G. Cahill, Rev. Sci. Instrum. **75**, 5119 (2004).
[12] A. J. Schmidt, Annu. Rev. Heat Transfer **16**, 159–181 (2013).
[13] Z. Cheng, T. Bai, Y. Wang, C. Li, K. D. Hobart, T. I. Feygelson, M. J. Tadjer, B. B. Pate, B. M. Foley, and L. Yates, ACS Appl. Mater. Interfaces **11**(20), 18517–18527 (2019).
[14] Z. Cheng, L. Yates, J. Shi, M. J. Tadjer, K. D. Hobart, and S. Graham, APL Mater. **7**, 031118 (2019).
[15] P. Jiang, B. Huang, and Y. K. Koh, Rev. Sci. Instrum. **87**, 075101 (2016).
[16] J. Liu, J. Zhu, M. Tian, X. Gu, A. Schmidt, and R. Yang, Rev. Sci. Instrum. **84**, 034902 (2013).
[17] Z. Cheng, A. Weidenbach, T. Feng, M. B. Tellekamp, S. Howard, M. J. Wahila, B. Zivasatienraj, B. Foley, S. T. Pantelides, and L. F. Piper, Phys. Rev. Mater. **3**, 025002 (2019).
[18] E. Chavez-Angel, N. Reuter, P. Komar, S. Heinz, U. Kolb, H.-J. Kleebe, and G. Jakob, Nanoscale Microscale Thermophys. Eng. **23**, 1 (2019).
[19] Z. Guo, A. Verma, X. Wu, F. Sun, A. Hickman, T. Masui, A. Kuramata, M. Higashiwaki, D. Jena, and T. Luo, Appl. Phys. Lett. **106**, 111909 (2015).
[20] M. D. Santia, N. Tandon, and J. Albrecht, Appl. Phys. Lett. **107**, 041907 (2015).
[21] J. Liu, Z. Xu, Z. Cheng, S. Xu, and X. Wang, ACS Appl. Mater. Interfaces **7**(49), 27279–27288 (2015).
[22] Z. Cheng, L. Liu, S. Xu, M. Lu, and X. Wang, Sci. Rep. **5**, 10718 (2015).
[23] Z. Cheng, Z. Xu, S. Xu, and X. Wang, J. Appl. Phys. **117**, 024307 (2015).
[24] P. Martin, Z. Aksamija, E. Pop, and U. Ravaioli, Phys. Rev. Lett. **102**, 125503 (2009).
[25] R. Wilson and D. G. Cahill, Phys. Rev. Lett. **108**, 255901 (2012).
[26] Z. Wang, J. E. Alaniz, W. Jang, J. E. Garay, and C. Dames, Nano Lett. **11**, 2206 (2011).
[27] A. Sood, J. Cho, K. D. Hobart, T. I. Feygelson, B. B. Pate, M. Asheghi, D. G. Cahill, and K. E. Goodson, J. Appl. Phys. **119**, 175103 (2016).
[28] C. Monachon, L. Weber, and C. Dames, Annu. Rev. Mater. Res. **46**, 433 (2016).
[29] R. Wilson, B. A. Apgar, W.-P. Hsieh, L. W. Martin, and D. G. Cahill, Phys. Rev. B **91**, 115414 (2015).
[30] Y. K. Koh, Y. Cao, D. G. Cahill, and D. Jena, Adv. Funct. Mater. **19**, 610 (2009).

Published under license by AIP Publishing